Eur. Phys. J. B **42**, 239–245 (2004)
DOI: 10.1140/epjb/e2004-00384-5

THE EUROPEAN PHYSICAL JOURNAL B

Inhomogeneous current distribution in wide high-temperature superconducting small-angle grain boundaries

K. Guth, V. Born, and Ch. Jooss[a]

Institut für Materialphysik, University of Göttingen, Friedrich-Hund-Platz 1, 37077 Göttingen, Germany

Received 6 August 2004
Published online 14 December 2004 –

Abstract. Using space resolved magneto-optical microscopy we have studied the development of the critical state in high temperature superconducting small-angle grain boundaries in magnetisation experiments. It has been found that with respect to the position in the grain boundary plane this critical state develops in a highly inhomogeneous manner. Towards the centre of the grain boundary there exists a distinct suppression of the inter-granular currents flowing across the grain boundary. A strong correlation between the static (critical current) and the dynamical properties (e.g. electric field or flux-line velocity) of the vortex system inside the grain boundary appears to be the principal mechanism for the observed inhomogeneous current distribution in wide bi-crystalline current bridges.

PACS. 74.25.Sv Critical currents – 74.72.Bk Y-based cuprates – 74.78.Bz High-T_c films – 74.81.Bd Granular, melt-textured, amorphous and composite superconductors

1 Introduction

Soon after the discovery of high temperature superconductivity in the cuprates [1], it has been found that in high-T_c materials, such as $YBa_2Cu_3O_{7-\delta}$ (YBCO), grain boundaries (GB) have a deleterious effect on the inter-granular transport properties. There has been a huge effort to quantitatively characterise this current suppression in bi-crystalline films. It has been found that the inter-granular critical current in bi-crystalline thin films decreases nearly exponentially with increasing grain boundary misorientation angle [2–6]. In addition, much fundamental and theoretical work has been done to understand the microscopic mechanisms of the observed current suppression in superconducting GBs [6–16]. The scope of almost all experimental studies in this field is to characterise and compare the superconducting properties of different bi-crystalline films to get a better understanding of the properties governing the exponential current suppression [6,7,14,15].

As transport measurements only give a mean value of the critical current averaged over the width of the sample (usually some few micrometres), there has been done only little work on the local distribution of the supercurrents in wide bi-crystalline current bridges [17]. Therefore, in this study we want to shed light onto open question, whether or not the supercurrents distribute themselves homogeneously over the width of a some hundred micrometre wide bi-crystalline current bridge and on the mechanisms which are involved. To solve this question, obviously a space resolved technique is needed to investigate the static and the dynamical properties of the flux distribution in magnetisation experiments. Magneto-optical (MO) imaging, an experimental technique for the visualisation of the flux- and current distributions in thin film superconducting samples [18,17,19], offers the unique possibility to study the current distribution in wide (some hundred micrometres) bi-crystalline samples with a spatial resolution of only some micrometres. Therefore, the MO microscopy is particularly suitable to study the local inter-granular current distribution in GBs.

In addition, in contrast to a four-probe measurement on a small test structure, where the vortex-vortex interactions are usually disregarded due to the very small width of the sample, the discussion of the experimental results of the MO microscopy on wide current bridges has to incorporate the influence of the large vortex system on the local current distribution in the GB. There are some MO studies of the local current density j_{gb} across thin film GB with very low misorientation angles (2° and 3°), where an increase of j_{gb} with the local flux density was observed [20–22]. This behavior was interpreted to be a result of the interaction of (weaker pinned) intergranular vortices with (stronger pinned) adjacent vortices in the grains. This behavior, however, changes in thin film small-angle GB with larger misorientation angle. As the reader will see later, in the studied current bridges, the inhomogeneous flux creep of the vortex ensemble near the

[a] e-mail: jooss@ump.gwdg.de

GB has a strong influence on the inter-granular current distribution inside the GB.

This aspect becomes more clear, if one considers for example the differences between a transport and a magnetisation measurement: In the transport measurement, due to the externally applied current, which is constantly driven across the GB, strong Lorentz forces act on the flux-lines inside the GB. Usually these experiments are performed at a voltage criterion of $U_c = 1\ \mu$V, but there exists no clear information about the realised local electric field during the transport measurement. Due to the disordered GB structure and the weakened superconducting properties one expects a much higher level of the electric field in the GB compared to the grains in this type of experiment. Contrarily, in magnetisation experiments, the currents are formed as screening currents due to the field sweep to a constant external magnetic field value. Here, the current distribution is mainly controlled by the interplay of the GB and bulk screening properties [23]. In addition, since there is no such external force that constantly drives the currents over the GB as in a transport experiment, in magnetisation experiments thermally activated flux creep may affect significantly the spatial distribution of the current density. Due to this relaxation process flux gradients can be reduced and the flux distribution evolves towards equilibrium with time [24]. Furthermore, geometrical or other constraints might lead to local differences in the relaxation rate, which result in inhomogeneities in the current- and electric field distributions.

With this in mind we made a deliberate study on the current distribution in superconducting small-angle tilt GBs in magnetisation experiments. To investigate the differences in the current distribution in homogeneous and bi-crystalline samples we used YBCO thin films grown on bi-crystalline $SrTiO_3$ substrates. Using MO imaging the local static and dynamical superconducting properties (flux distribution, critical current density and flux velocity) have been analysed inside and far off the GB. A model for the vortex motion in the GB area is presented and compared with experimental results for the static and the dynamical properties of superconducting GBs.

2 Experimental

Superconducting c-axis oriented YBCO thin films were grown on bi-crystalline $SrTiO_3$ substrates with pulsed laser deposition using a KrF excimer laser ($\lambda = 245$ nm). The repetition rate was 6 Hz and the energy density on the target's surface 1.8 Jcm^{-2}. The oxygen pressure was 0.6 mbar and the substrate temperature has been kept constant at 760 °C during the ablation process. As a final step, the films were in-situ oxygenated at 400 °C and 750 mbar for about 30 minutes. For magneto-optical imaging 750 μm wide superconducting tracks were patterned by optical lithography and wet chemical etching.

The subsequent characterisation of the films' superconducting properties has been performed in a magneto-optical polarisation microscope. All magnetic field distributions that are presented in this paper are measured by means of quantitative MO microscopy in a helium flow cryostat at 8 K [17,25]. Except Figure 3b the current distributions are magnetisation or screening currents generated by an external magnetic field. Applied fields ranged from 1 mT up to 200 mT. The experimental setup consist of an iron garnet film that is firmly pressed onto the patterned YBCO sample. The field sensing iron garnet is observed via a polarisation microscope using a power stabilised light source. The polariser-to-analyser position is optimised to maximum contrast and is usually near 90°. Light intensity distributions representing the magnetic field distribution $B_z\ (x, y)$ are recorded with a commercial CCD camera using exposure times of 10 μs to 250 μs. B_z values are mapped to the recorded grey scales using a non-linear calibration function determined for each sample separately. Current distributions were then calculated using an inversion scheme for Biot-Savart's law, which gives an integral relation between the measured magnetic field B_z and the current distribution within the sample [18,17]. For the calculated currents a spacial resolution of approximately 3–5 μm is achieved.

The study of inhomogeneous intergranluar current density distributions is based on a set of more than 25 bi-crystalline films with symmetric [001] tilt boundaries and tilt angles between 3° and 16°. In the following, our typical findings are presented examplarly for 4° and 6° tilt GB.

3 Results

Figure 1 shows a grey-scale image of the flux distribution in a bi-crystalline YBCO thin film with a symmetrical 4° [001] tilt boundary (lying horizontally in the image) in an external magnetic field of $B_{ext} = 92.2$ mT. In this picture dark regions represent low and bright regions high values of B_z . The current distribution, as calculated by the inversion of Biot-Savart's law [18], is indicated as a white contour line pattern within the image. Current profiles for the inter- (Fig. 1a) and intra-granular current distributions (Fig. 1b) are taken along the horizontal lines in the grey-scale representation.

As can be easily seen, there exists a nearly homogeneous distribution of the intra-granular current density $j_c = 3.9 \pm 0.4 \times 10^{11}$ A/m^2 in the undisturbed region of the sample (Fig. 1 b). This corresponds to a variation in j_c over the width of the sample of 20%, which marks the maximum spread in j_c that has been observed in a large number of samples. Generally, in most of the studied samples we find a nearly constant j_c not varying more than 10% over the width of the current bridge, which corresponds to the accuracy of the inversion scheme for the flux distributions [17]. In contrast to this, we find a highly inhomogeneous current-distribution for the inter-granular currents at the GB. Here, a distinct suppression of the current density towards the interior of the GB plane of more than 50% can be detected (see the dotted lines in Fig. 1a for reference). It has to be pointed out that the pronounced maxima in j_{gb} at the sample's edges are caused by the coupling of the in-plane component of the magnetic

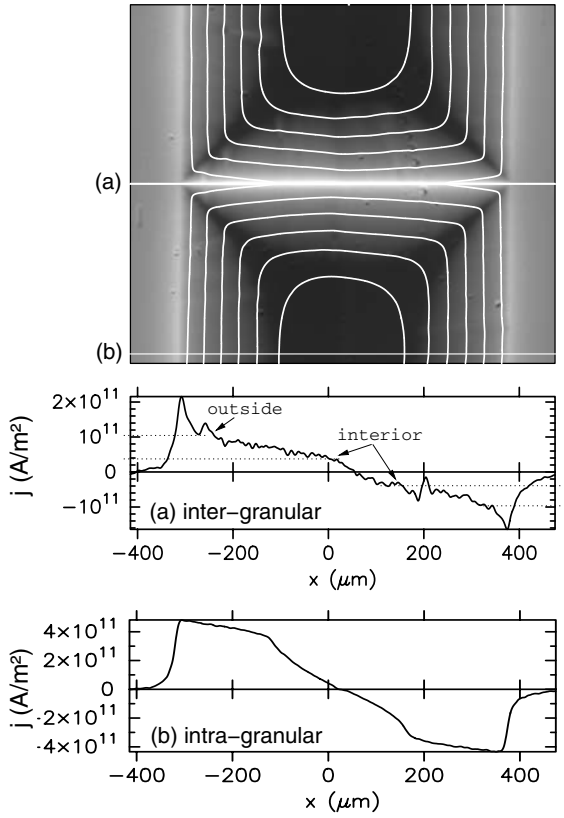

Fig. 1. Flux- and current distribution in the *partly penetrated* state in a bi-crystalline YBCO film with a symmetrical 4° [001] tilt boundary. The external magnetic field $B_{\rm ext}$ is 92.2 mT. Bright corresponds to high B_z values. The current profiles are taken along the two horizontal lines within the image. In (a) the inter-granular current distribution is displayed, whereas (b) shows the intra-granular currents. The dotted lines in (a) mark the reduction of $j_{\rm gb}$ towards the centre of the GB plane.

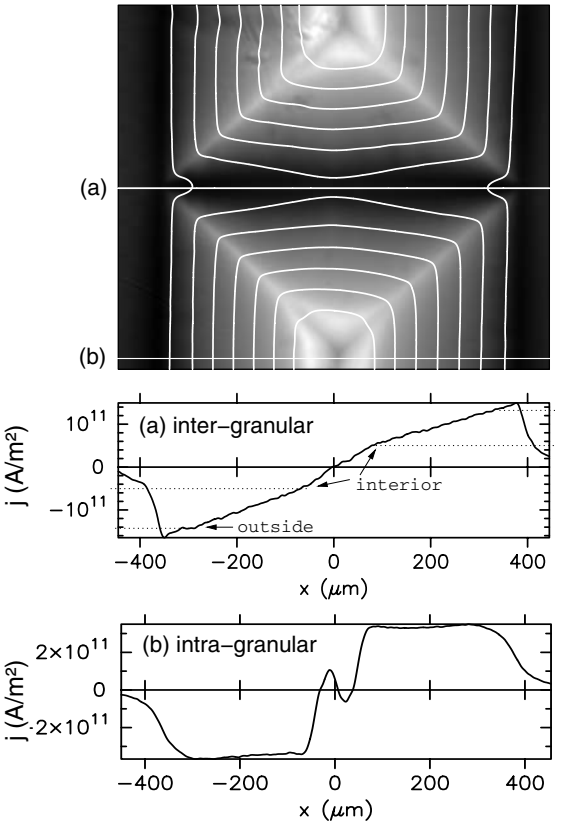

Fig. 2. Flux- and current distribution in the *remanent* state in the same bi-crystalline YBCB film with a symmetrical 4° [001] tilt boundary as in Figure 1. The maximum external magnetic field $B_{\rm max}$ for nearly full penetration was 250 mT. Bright corresponds to high B_z values. The current profiles are taken along the two horizontal lines within the image. In (a) the inter-granular current distribution is displayed, whereas (b) shows the intra-granular currents. The dotted lines in (a) mark the reduction of $j_{\rm gb}$ towards the centre of the GB plane.

field B to the magnetisation of the field sensing iron garnet layer [26]. Therefore, we usually exclude these maxima from the evaluation of $j_{\rm gb}$. Doing so, we find a range of $j_{\rm gb}$ from $j_{\rm gb} \approx 10 \times 10^{10}\,{\rm A/m^2}$ in the outer parts of the GB to $j_{\rm gb} \approx 4.5 \times 10^{10}\,{\rm A/m^2}$ in the interior for the sample presented in Figure 1a. For clarity reasons, the different levels of $j_{\rm gb}$ are indicated by the dotted lines in Figure 1a.

In the remanent state with a vanishing external magnetic field $B_{\rm ext} = 0$ mT, these features are even more striking than in the partly penetrated state. Figure 2 displays the remanent flux- and current distribution in the same bi-crystalline sample as in Figure 1. The maximum applied external field $B_{\rm max}$ for nearly full penetration was 250 mT. In comparison to the partly penetrated state one can clearly see the inversion of the current-flow direction due to the remanent magnetisation currents. Again, an almost constant intra-granular current density of $j_{\rm c} = 3.7 \pm 0.2 \times 10^{11}\,{\rm A/m^2}$ appears over the whole width of the sample (Fig. 2b).

In this experiment it becomes even more obvious that there exists no systematic spatial variation in $j_{\rm c}$ for the homogeneous parts of the sample far-off the GB. With respect to the suppression of the inter-granular currents along the GB plane we find a nearly linear decrease of $j_{\rm gb}$ towards the sample's centre in the remanent state (Fig. 2a). In fact, $j_{\rm gb}$ decreases from its maximum value of about $11 \times 10^{10}\,{\rm A/m^2}$ in the outer part of the GB to $5 \times 10^{10}\,{\rm A/m^2}$ in the GB's centre. This is again a drop in $j_{\rm gb}$ of more than 50%.

It is necessary to point out that this observed inhomogeneous current pattern across the GB is typical for all bi-crystalline films with tilt angles larger than 4°. It is also independent of the magnetic history of the sample. This can be seen by comparing current distributions in increasing and decreasing external magnetic field in Figures 1 and 2. Consequently, a local magnetic field dependence $j_{gb}(B)$ can be ruled out to be the main reason for the observed spatial dependence of the intergranular current density. This is in contrast to bi-crystalline films with very low misorientation angles, where a clear dependence of j_{gb} on the magnetic history was found [20].

It has to be pointed out that except Figure 3b all current distributions presented in this paper are

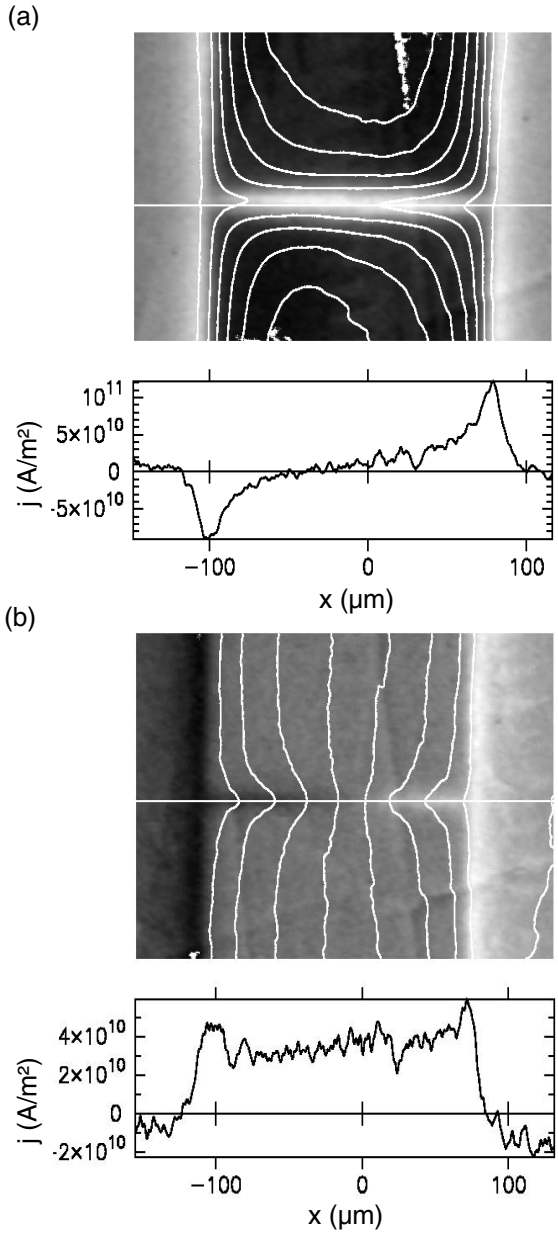

Fig. 3. Magneto-optical imaging of a transport and a magnetisation experiment with a 6° [001] bi-crystalline YBCO thin film. The images show the flux distribution as a grey scale pattern. The current profiles are taken along the GB. The inter-granular currents for the magnetisation experiment is shown in (a) and for the transport case in (b).

magnetisation currents. In this case a current distribution induced by an external magnetic field develops within the superconducting sample in accordance to the superconducting critical state. In comparison to transport measurements, there exists no external force that actively drives the magnetisation currents across the GB, creating a highly dissipative state. As a result, the observed inter-granular currents cannot be compared directly to results from transport experiments, since here a different non-equilibrium state with lower electric field values is realised which correspond to a much smaller voltage criterion U_c. The observed over-all current distribution rather represents the system-answer to the external magnetic field (or magnetic field history), i.e. the current distribution that results from a minimisation of the dissipation and the acting Lorentz forces for the magnetic field screening in the grains and the GB. Therefore, a comparison of transport and magnetisation experiments is a crucial task and cannot easily be done with data from the literature. But a comparison of transport- and magnetisation MO is well possible [27]. In Figure 3 we present a comparison of a magnetisation- (Fig. 3a) and a transport (Fig. 3b) experiment on a bi-crystalline YBCO thin film with a symmetrical 6° [001] tilt boundary. The external field of about 16 mT in the magnetisation experiment was chosen in that way, that the flux pattern inside the GB closely matches the one in the transport case. In both images we find the GB completely filled with flux, while the adjacent grains are still almost flux free. This fact reflects the strong current suppression in the case of a 6° [001] tilt boundary compared to the intra-granular critical current. In fact, the inter-granular currents are more than one order of magnitude smaller than the intra-granular ones. In addition, we find clear differences in the local distribution of the currents inside the GB. While the magnetisation currents again distribute very inhomogeneously over the width of the GB, the transport currents reach an almost constant value of j_{gb} throughout the whole GB plane, and thus seem to be in accordance with the static Bean model. This supports the idea that for the transport currents, the level of dissipation is externally fixed in the GB plane by the applied voltage criterion, while in the other case the relaxation rate of the magnetic field distribution dominates the current distribution in the GB.

Based on these experimental studies we think that for the understanding of this highly inhomogeneous current distribution in wide bi-crystalline current bridges in magnetisation experiments, a simple description of the static vortex system is not sufficient to explain the observed properties. Moreover, in our opinion the dynamical properties of the corresponding flux-line lattice play an important role in the occurrence of the observed declining inter-granular current distribution. And thus, the total inter-granular critical current distribution reflects the interplay of the development of a Bean-like critical state and the thermally activated flux dynamics within the sample.

To get a deeper insight into the mechanisms governing the current distribution in bi-crystalline thin films in magnetisation experiments we start from the current distribution as it is given by the Bean model. Figure 4 shows a schematic overview of the static Bean-like current distribution in a superconducting bi-crystalline thin film. Under the assumption of constant intra- and inter-granular critical currents, we find a pattern of parallel current stream lines, that bend towards the sample's centre in the vicinity of the GB. This fact is just an expression of the reduced inter-granular currents j_{gb} compared to the intra-granular ones. At the bending points of the currents, that are also present in the sample's corners, so-called discontinuity

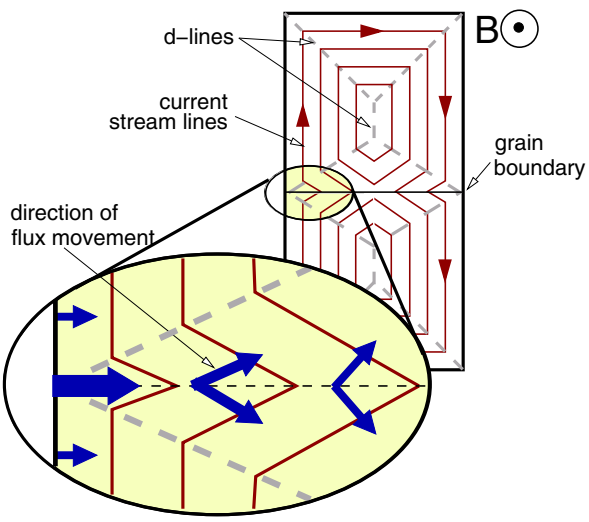

Fig. 4. Dynamical properties of the flux distribution: Bean-like current distribution in a bi-crystalline superconducting thin film. The superconducting currents are represented by the parallel current-flow lines. The dashed grey lines show the double-*Y* pattern of the discontinuity lines (d-lines) formed in a bi-crystalline thin film. In addition to the static treatment of the Bean model, the enlarged GB segment explains the direction of flux movement due to thermally activated relaxation processes in a magnetisation experiment with an external applied field. This representation of the flux velocity extends the static Bean model by a dynamical treatment of the flux-line system.

lines (*short*: d-lines) are formed. There are five d^+-lines present in each grain that form a double-Y pattern. These d^+-lines separate current domains with constant j_c but different current flow direction. In addition, there exists one d^--line at the GB, where we find an additional change in the magnitude of the supercurrents.

Now, in contrast to the Bean model, that assumes constant critical currents in the whole GB as well as a static flux-line lattice we find a decreasing inter-granular critical current towards the sample's centre inside the GB. As mentioned previously, the flux creep model [24] allows for such a local current suppression in homogeneous, bi-crystalline thin films. This flux creep leads to a progressive reduction of the non-equilibrium critical state in the GB. The movement of the flux-lines is always directed perpendicular to the supercurrents and the magnetic field direction. Thus, in the set-up of a partly penetrated state the flux-lines move towards the sample's centre, as indicated in Figure 4. It is easy to understand that at the d^+-lines flux-lines from different current domains will meet. But as a result of the repulsive flux-line–flux-line interaction, in the Bean model these flux quanta cannot cross the d^+-lines. Thus, the d^+-lines form so-called boundaries for the flux movement. Considering the GB area in more detail, one finds that the four d^+-lines above and below the GB intersect with the GB plane at the sample's edges. This leads to a geometrical boundary condition for the flux movement that is described best by the air flow in a jet engine. Due to the small opening of the d^+-lines in the outer parts of the GB near the sample's edge the flux-lines are accelerated with a velocity component strictly parallel to the GB plane (see Fig. 4). Moving further into the sample's centre, this boundary condition is more and more relaxed and the flux-lines start to distribute into the adjacent GB current domains, reducing the non-equilibrium state in the GB plane, that was created by the applied external field. This leads to a smaller flux-line velocity parallel to the GB plane. In other words, in comparison to the GB's centre we find a dissipative state of the flux-line lattice in the outer parts of the GB reflecting the less relaxed state in this region. In connection with the non-equilibrium critical state we expect larger flux-line velocities, higher electric field values and larger critical currents in this area. On the other hand, we suppose that in the central region of the GB we have a much faster relaxation rate due to the possibility to redistribute the flux into the adjacent current domains. And as a result of the faster relaxation process, we find lower levels of the electric field and a reduced critical current density in this quickly relaxing region of the GB. With respect to the representation in Figure 4 it is important to note that since the flux velocity is always perpendicular to the direction of the currents, the current distribution (especially the orientation of the current flow direction) will be modified by the discussed relaxation process. We find this deviation from the Bean-like current distribution in our experiments. For clarity reasons, in the image we have used the current distribution following from the Bean model. In contrast to the experiments, this leads to an angle $\alpha \neq 90°$ between the flux velocity and the currents in the enlarged GB segment of Figure 4.

In sum, due to geometrical boundary conditions we have a coexistence of differently fast relaxing regions of the flux-line lattice in the GB that theoretically explains the observed inhomogeneities in the inter-granular current distribution.

To further support the idea of different relaxation rates in the GB, we have performed time resolved magneto-optical imaging to study the relaxation process of the flux-distribution in a bi-crystalline thin film sample. In combination with the inversion of Biot-Savart's law this technique offers the possibility to investigate the time dependent relaxation of the flux- and current distribution ($\Delta \boldsymbol{B}(t)$ and $\Delta \boldsymbol{j}(t)$) at the same time. These two experimental quantities form the basis for a quantitative investigation of dynamical properties of the flux-distribution in magnetisation experiments. Starting from the measured $\Delta \boldsymbol{B}(t)$ and $\Delta \boldsymbol{j}(t)$ values, it is possible to calculate the two-dimensional inductive electric field distribution $\boldsymbol{E}^{\mathrm{ind}}$ from Maxwell's equation $\partial_t \boldsymbol{B} = -\nabla \times \boldsymbol{E}^{\mathrm{ind}}$ in the limit of a two-dimensional approximation. Within this approximation, the electric field component normal to the film surface is disregarded. From the observation that the direction of the obtained in-plane components of $\boldsymbol{E}^{\mathrm{ind}}$ deviates from the direction of the in-plane current density, the total electric field $\boldsymbol{E}^{\mathrm{tot}}(x,y) = \boldsymbol{E}^{\mathrm{pot}} + \boldsymbol{E}^{\mathrm{ind}}$ can be infered, where the potential part of the electric field is

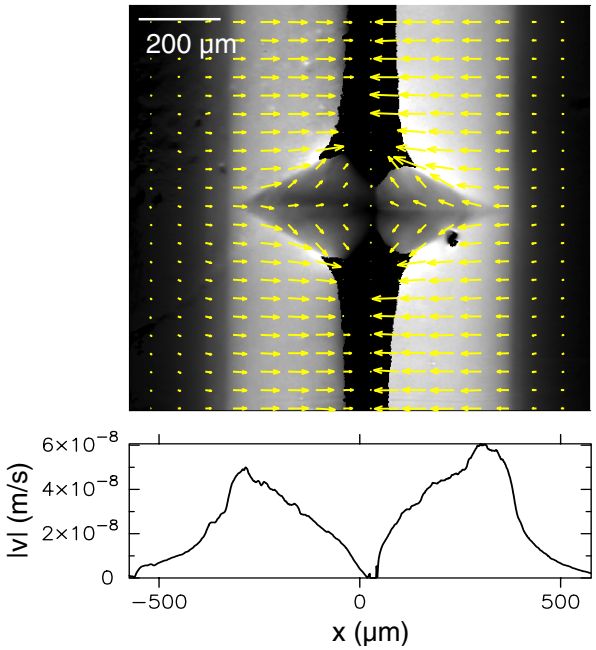

Fig. 5. Mean flux-line velocity in a bi-crystalline YBCO film with a 3° [001] tilt boundary in a partly penetrated state. The vectors indicate the direction and the magnitude of the flux-line velocity $\boldsymbol{v}$. The experimental details for the time resolved MO imaging were as follows: External field $B_{\rm ext}$ =132 mT, time resolution Δt=14.6 s, first image was taken at t_1=2.4 s after the application of $B_{\rm ext}$. The dark spot on the right side of the image just below the GB is caused by a blind region of the indicator.

realted to the induced charge density via $\nabla \cdot \boldsymbol{E}^{\rm pot} = \epsilon_0 n^{in}$. In a further step, the dissipated power density ($|\boldsymbol{p}| = |\boldsymbol{E}^{\rm tot} \cdot \boldsymbol{j}|$) and the mean flux-line velocity ($\boldsymbol{E} = -\boldsymbol{v} \times \boldsymbol{B}$) can be extracted from the evaluated data. For a full description of the electric field imaging technique by MO microscopy and a more detailed analysis of the dynamical properties of the magnetic field distribution in high temperature superconducting thin films we refer to references [19,28].

Here, we want to focus on the mean flux-line velocity as calculated by the presented method. It has to be pointed out that with respect to the limited resolution of the MO imaging system, the presented $\boldsymbol{B}$, $\boldsymbol{j}$ and $\boldsymbol{v}$ distributions have a maximum resolution of about 3–5 μm. Therefore, the description on the basis of thermally activated relaxation processes in the GB as well as the measured velocity distribution represent a description of the mean flux-line velocity or the motion of so-called flux bundles, and not of single vortices. As can be seen in Figure 5 we find exactly the same maximum of the flux velocity $\boldsymbol{v}$ in the GB near the edges of the current bridge as proposed in the previous part of this paper. This maximum in $\boldsymbol{v}$ represents the non-equilibrium state in this region discussed above and is directly related to the higher level of dissipation caused by the fast motion of the flux-lines. Moving towards the centre of the GB plane we find a reduction of the mean flux line velocity by nearly a factor of ten. Furthermore, in accordance to our model it is visible that the angle between the flux velocity and the GB plane increases towards the GB's centre (see the vector field in Fig. 5). This clearly supports the idea of a redistribution of the flux into the adjacent GB current domains as the opening of the d^+-lines becomes wider, while moving from the sample's edge towards the centre of the GB.

4 Summary

Here, we have presented a detailed study of the static and dynamical properties of the flux- and current distribution in bi-crystalline YBCO thin film samples. The focus of our study was on the homogeneity of the inter-granular current distribution inside the GB. We have shown that in contrast to transport experiments the magnetisation currents distribute inhomogeneously over the width of the GB. Strictly speaking, we have found a strong decrease of $j_{\rm gb}$ towards the GB's centre in magnetisation experiments. To explain this experimental current distribution, that clearly deviates from the one that is expected by the static Bean model, we analysed the dynamical properties of the flux-line lattice with respect to the mean flux-line velocity inside the GB. In accordance to our time resolved experiments, where we found a minimum of the flux-line velocity in the GB's centre, we have developed a model, that describes the differently fast reduction of the non-equilibrium state in the inner and the outer parts of the GB.

In summary, we have shown, that in magnetisation experiments geometrical constrains, such as the discontinuity lines, lead to a current distribution that clearly deviates from the static Bean-like current distribution in superconducting bi-crystalline thin films.

One of the authors would like to thank H.U. Krebs for the use of the laser ablation facility. This work was supported by the Deutsche Forschungs Gemeinschaft (DFG).

References

1. J.G. Bednorz, K.A. Müller, Z. Phys. B **64**, 189 (1986)
2. D. Dimos, P. Chaudhari, J. Mannhart, F.K. LeGoues, Phys. Rev. Lett. **61**, 219 (1988)
3. D. Dimos, P. Chaudhari, J. Mannhart, Phys. Rev. B **41**, 4038 (1990)
4. Z.G. Ivanov, P.A. Nilsson, D. Winkler, T. Claeson, E.A. Stepntsov, A.Y. Tzalenchuk, Appl. Phys. Lett. **59**, 3030 (1991)
5. N.F. Heinig, R.D. Redwing, J.E. Nordman, D.C. Larbalestier, Phys. Rev. B **60**, 1409 (1999)
6. H. Hilgenkamp, J. Mannhart, Rev. Mod. Phys. **74**, 485 (2002)
7. M.A. Schofield, M. Beleggia, Y. Zhu, K. Guth, Ch. Jooss, Phys. Rev. Lett. **92**, 195507 (2003)
8. J. Mannhart et al., Philos. Mag. B **80**, 827 (2000)

9. H. Hilgenkamp, J. Mannhart, Appl. Phys. Lett. **73**, 265 (1998)
10. H. Hilgenkamp, C.W. Schneider, R.R. Schulz, B. Goetz, A. Schmehl, H. Bielefeldt, Physica C **326–327**, 7 (1999)
11. S.E. Babcock, J.L. Vargas, Annu. Rev. Mater. Sci. **25**, 193 (1995)
12. N. Browning, J. Buban, P. Nellist, D. Norton, M. Chisholm, S. Pennycook, Physica C **294**, 183 (1998)
13. S.E. Babcock, D.C. Larbalestier, J. Phys. Chem. Solids **55**, 1125 (1994)
14. M. Chisholm, M. Pennycook, Nature **351**, 47 (1991)
15. A. Gurevich, E. Pashitskii, Phys. Rev. B **57**, 13878 (1998)
16. A. Gurevich, Phys. Rev. B **48**, 12857 (1993)
17. Ch. Jooss, J. Albrecht, H. Kuhn, S. Leonhardt, H. Kronmüller, Rep. Prog. Phys. **65**, 651 (2002)
18. Ch. Jooss, R. Warthmann, A. Forkl, H. Kronmüller, Physica C **299**, 215 (1998)
19. Ch. Jooss, E. Brinkmeier, V. Born, W. Westhäuser, K. Guth, in *Magneto-Optical Imaging*, Vol. 1 of NATO Science Series, edited by T.H. Johansen, D.V. Shantsev (Kluwer Academic Publishers, Holland, 2004), p. 29
20. J. Albrecht, S. Leonhardt, H. Kronmüller, Phys. Rev. B **63**, 014507 (2000)
21. Ch. Jooss, J. Albrecht, Z. Metallkd **93**, 1065 (2002)
22. J. Albrecht, Phys. Rev. B **68**, 054508 (2003)
23. V. Born, K. Guth, H.F. Freyhardt, Ch. Jooss, Supercond. Sci. Technol. **17**, 380 (2004)
24. M.R. Beasley, R. Labusch, W.W. Webb, Phys. Rev. **181**, 682 (1969)
25. K. Guth, V. Born, C. Brandt, S. Sievers, H.C. Freyhardt, Ch. Jooss, Supercond. Sci. Technol. **17**, 65 (2004)
26. T.H. Johansen et al., Phys. Rev. B **54**, 16264 (1996)
27. A.V. Bobyl, D.V. Shantsev, Y.M. Galperin, T.H. Johansen, M. Baziljevich, S.F. Karmanenko, Supercond. Sci Technol. **15**, 82 (2002)
28. Ch. Jooss, V. Born, W. Westhäuser, submitted